Materials Research Bulletin 95 (2017) 509–514

Contents lists available at ScienceDirect

Materials Research Bulletin

journal homepage: www.elsevier.com/locate/matresbu

Tunable phase and upconverting luminescence of Gd^{3+} co-doped $NaErF_4$:Yb^{3+} nanostructures

Wanying Xie[a], Xitao An[a,b], Li Chen[a,c,*], Jing Li[c], Jing Leng[c], Wei Lǔ[d], Ligong Zhang[e], Yongshi Luo[e]

[a] School of Chemical Engineering & Advanced Institute of Materials Science, Changchun University of Technology, 2055 Yan'an Street, Changchun, Jilin, 130012, China
[b] School of Chemistry and Life Science, CCUT, 2055 Yan'an Street, Changchun, China
[c] School of Basic Sciences, CCUT, 2055 Yan'an Street, Changchun, China
[d] School of Materials Science and Engineering, CCUT, 2055 Yan'an Street, Changchun, China
[e] State Key Laboratory of Luminescence and Applications, CIOMP, CAS, Changchun, China

ARTICLE INFO

Keywords:
Upconversion luminescence
NaErF4:Yb3+ nanoparticles and nanorods
Transient spectroscopy
Gd3+-codoping

ABSTRACT

Upconverting $NaErF_4$:Yb^{3+},Gd^{3+} nanoparticles (NPs) and nanorods (NRs) with improved red emission have been successfully achieved *via* a facile hydrothermal route using oleic acid as the assistant surfactant. The crystalline phase, morphology even the size are simultaneously tuned by controlling the reaction temperatures and Gd^{3+} doping contents. The higher synthesis temperature leads to the morphology evolution from NPs to NRs. The integrated intensity ratio of red to green emissions is much improved for Gd^{3+} codoping nanostructures. The microstructure characterizations along with the steady and transient spectroscopy are performed to better understand the underlying mechanisms of phase evolution and emission enhancement. For the different states of Er^{3+}, *i.e.* $^2H_{11/2}$ and $^4F_{9/2}$, the radiative/non-radiative transition probabilities could be affected by Gd^{3+} doping in different ways as for NPs and NRs, based on the lifetime and emission intensity data. $NaErF_4$:Yb^{3+},Gd^{3+} nanosctructures are expected to have promising applications in multimodal bioimaging for deeper tissue penetration.

1. Introduction

Recently, lanthanide-doped upconversion nanocrystals (UCNCs) have attracted increasing interest due to their potential applications in various domains of biological probes, *in vivo* imaging, solar cells and color displays [1–8]. Compared to the conventional fluorescent probes such as organic dyes and quantum dots, UCNCs possess some unique advantages in terms of the tissue penetration depth, weak background autofluorescence, excellent physical and chemical stability and low cytotoxicity [9–11]. Moreover, the fluoride is generally considered as an optimal host matrix owning to its low phonon energy, high upconversion efficiency, enhanced resistance to photobleaching [12–14]. In comparison with the most widely used Y-based compounds (*e.g.* $NaYF_4$:Yb,Er) [15,16], Er-based host matrix favors the intense red emissions, which is more beneficial to the *in vivo* bioimaging because of their low tissue absorption [17]. In addition, appropriate content of Yb^{3+}, an efficient sensitizer, can remarkably enhance upconversion emissions by taking advantage of its large absorption cross-section for 980 nm excitation wavelength and efficient energy transfer to Er^{3+} [18–20]. As in the previous reports, Gd^{3+} can be used as an intermediary to promote the energy transfer of fluoride due to the far distance between the first excited state level ($^6P_{7/2}$) and the ground level ($^8S_{7/2}$) of Gd^{3+} 4*f* electron configuration [21,22]. Extensive efforts have been devoted into controllable synthesis of lanthanide-doped UCNCs with homogeneous size/phase distribution and better dispersity besides the high upconversion efficiency to meet the growing demand of biological applications. Among most of the techniques, hydro/solvothermal approach proves to be a most effective and convenient one for cubic or hexagonal fluoride nanocrystals with various shapes and sizes [23]. The reduction in UCNCs size has been achieved in $NaYF_4$:Yb,Er systems *via* introducing of Gd^{3+} into the crystalline lattices [24]. Meanwhile, the reaction temperature also plays a significant role in the morphology evolution of the final products [25]. A few achievements have been reported so far the successful synthesis of β-$NaYF_4$:Yb, Er/Tm NCs with bright green fluorescence [26]. Ding and colleagues have precisely controlled the growth of β-$NaYF_4$:Yb, Er microcrystals and simultaneously provided a reference for exploration of the morphology-dependent UC luminescence properties [27]. However, as far as we know up to date, very few research have been reported on phase-controlled synthesis of Yb^{3+}, Gd^{3+} co-doped $NaErF_4$ UCNCs with improved UC

* Corresponding author at: School of Basic Sciences & Advanced Institute of Materials Science, Changchun University of Technology, 2055 Yan'an Street, Changchun, Jilin, 130012, China.
E-mail address: chenli@ccut.edu.cn (L. Chen).

http://dx.doi.org/10.1016/j.materresbull.2017.08.033
Received 17 June 2017; Received in revised form 12 August 2017; Accepted 13 August 2017
Available online 18 August 2017

luminescence.

In this contribution, $NaErF_4:Yb^{3+}$ and $NaErF_4:Yb^{3+},Gd^{3+}$ nanocrystals with various morphologies were synthesized *via* a facile hydrothermal process. The effects of reaction temperature and Gd^{3+} doping content on the crystalline phase, size and upconversion luminescence have been investigated in detail. Steady state and transient spectroscopy measurements were performed to better understand the mechanisms of enhanced luminescent properties after doping Gd^{3+}. The possible formation mechanism for the phase and morphology evolution was also discussed.

2. Experimental

2.1. Materials

$RE(NO_3)_3$ (RE = Er, Yb and Gd) solutions are freshly prepared by dissolving RE_2O_3 in nitric acid. RE_2O_3 (purity > 99.9%) and Oleic acid (OA, 90%) are purchased from Sigma-Aldrich. NaF, NaOH, and HNO_3 are supplied by Sinopharm Chemical Reagent Co., Shanghai, China. All of the other chemical reagents are analytical grade and used directly without further purification.

2.2. Synthesis of $NaErF_4:Yb^{3+}$, Gd^{3+} UCNCs

$NaErF_4$: 30%Yb^{3+}/xGd^{3+} (x = 0, 25 mol%) UCNCs were prepared by a hydrothermal route using oleic acid (OA) as the capping ligand and surfactant as previously reported [28]. At first, 10 mL anhydrous alcohol and 3 mL deionized water containing 1.2 g of NaOH were mixed under stirring to form a homogeneous solution, then followed by adding 20 mL OA to form a sodium-OA complex. As presented in Table 1, 1 mmol $RE(NO_3)_3$ with designed molar ratios and 8 mmol NaF were added into aforementioned solution with vigorously stirring at room temperature for 20 min. Subsequently, the gelatinous solution was sealed in a 50 mL Teflon-lined stainless autoclave, which was continuously heated at a particular temperature (Table 1) for 12 h. After the reaction, the system was cooled down to the room temperature naturally. The obtained precipitates were isolated by centrifugation at 10,000 rpm for 10 min, washed three times with ethanol and deionized water in sequence to remove the residue of organic ligands and other mixtures on the samples, and finally dried in vacuum oven at 60 °C for 10 h.

2.3. Characterization

The X-ray powder diffraction (XRD) patterns of the as-prepared samples were measured on a Rigaku D/Max IIA with Cu Kα radiation (λ = 1.54056 Å). The scan range was set from 10 to 70° with the scanning rate of 6.0°/min. The morphologies of the nanocrystals were obtained by using a transmission electron microscope (TEM, JEM-2000EX) operating at an acceleration voltage of 200 KV. Photoluminescence spectra were recorded by using a spectrophotometer (Hitachi F-7000) under external excitation of a CW 980 nm diode laser. The decay curves are detected by a Triax 550 spectrometer (Jobin-Yvon) and recorded using a Tek-tronix digital oscillters (TDS 3052), while a pulsed laser of 10 ns with tunable wavelengths from an optical parametric oscillator (OPO) pumped by a Nd: YAG laser (Spectraphysics, GCR 130) is used as an excitation source. All the measurements were performed at room temperature.

Table 1
Summary of the composition of nanocrystals, synthesis temperature (T), and morphologies of the samples.

Samples	Composition	T (°C)	Morphology
S1	$NaErF_4$: 30%Yb^{3+}	140	NPs
S2	$NaErF_4$: 30%Yb^{3+}/25%Gd^{3+}	140	NPs
S3	$NaErF_4$: 30%Yb^{3+}	190	NRs
S4	$NaErF_4$: 30%Yb^{3+}/25%Gd^{3+}	190	NRs

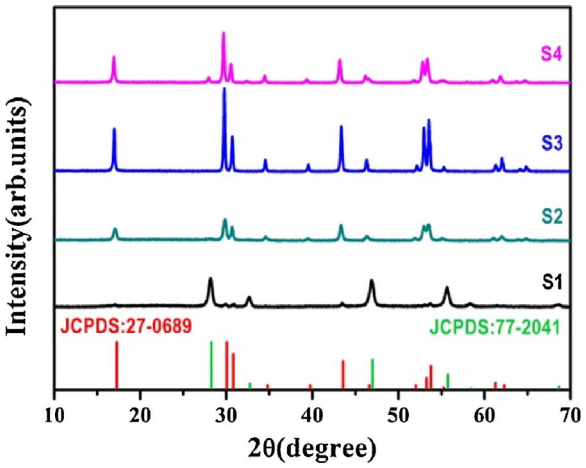

Fig. 1. XRD patterns of as-prepared samples. S1:$NaErF_4$: 30%Yb^{3+} NPs; S2: $NaErF_4$: 30% Yb^{3+}/25%Gd^{3+} NPs; S3: $NaErF_4$: 30%Yb^{3+} NRs; S4: $NaErF_4$: 30%Yb^{3+}/25%Gd^{3+} NRs.

3. Results and discussions

Fig. 1 shows the XRD patterns of the as-prepared $NaErF_4$: 30%Yb^{3+} nanocrystals along with 25 mol% Gd^{3+} co-doped samples at different synthesis temperatures. When the reaction temperature was 140 °C, the Gd^{3+}-free sample matched perfectly with standard cubic phase $NaErF_4$ (JCPDS No: 77-2041), demonstrating that pure cubic phase nanoparticles can be obtained at lower reaction temperature. At the Gd^{3+} doping concentration of 25%, the crystal phase of UCNCs transforms from cubic phase to hexagonal phase completely. In current host lattice of $NaErF_4$, Gd^{3+} (r = 1.193 Å) is rationally considered to replace Er^{3+} (r = 1.144 Å) owing to the identical charge valence. Importantly, lanthanides with larger ionic radius show a higher trend towards electron cloud distortion due to increased dipole polarizability, and thus preferably induce the hexagonal structures. Similar expanding effects in unit-cell volume as well as interplanar distance resulting from dopant ions with larger radius than substituted ions have been reported in Gd^{3+} doped $NaYF_4$ nanocrystals [29]. In the case of the reaction temperature of 190 °C, all of the diffraction peaks of $NaErF_4$: 30%Yb^{3+} were found to be in good agreement with the standard hexagonal phase $NaErF_4$ (JCPDS No: 27-0689), indicating that single hexagonal phase nanorods with good crystallinity were formed. And the diffraction peaks of $NaErF_4$: 30%Yb^{3+}/25%Gd^{3+} nanorods mainly present the hexagonal phase. Simultaneously, the diffraction peak shifts slightly towards the lower-angle side because of the expansion in unit-cell volume and interplanar distance attributed to the substitution of Er^{3+} ions by larger radius Gd^{3+} in the host lattice. We also noticed that the diffraction peaks get broadened by doping Gd^{3+} ions, revealing the shrinkage of the average crystalline size. It is noteworthy that as the synthesis temperature was increased up to 190 °C, the crystalline phase of $NaErF_4$: 30%Yb^{3+} converts from cubic to hexagonal (see the XRD patterns of S1 and S3 shown in Fig. 1). Compared with the high-temperature metastable cubic phase, the hexagonal phase is more stable thermodynamically. Therefore, synthesizing the hexagonal phase UCNCs needs excess thermal energy to overcome the higher energy barrier. Such growth processes of $NaYF_4$ nanocrystals governed by thermodynamics have been already documented [30]. It is reasonable to believe that reaction temperature is highly important for the phase control of the $NaErF_4$: 30%Yb^{3+} nanocrystals.

Fig. 2 presents the transmission electron microscopy (TEM) and selected area electron diffraction (SAED) images illustrating the morphology/phase evolution of the samples synthesized under the conditions listed in Table 1. The typical TEM images show the excellent

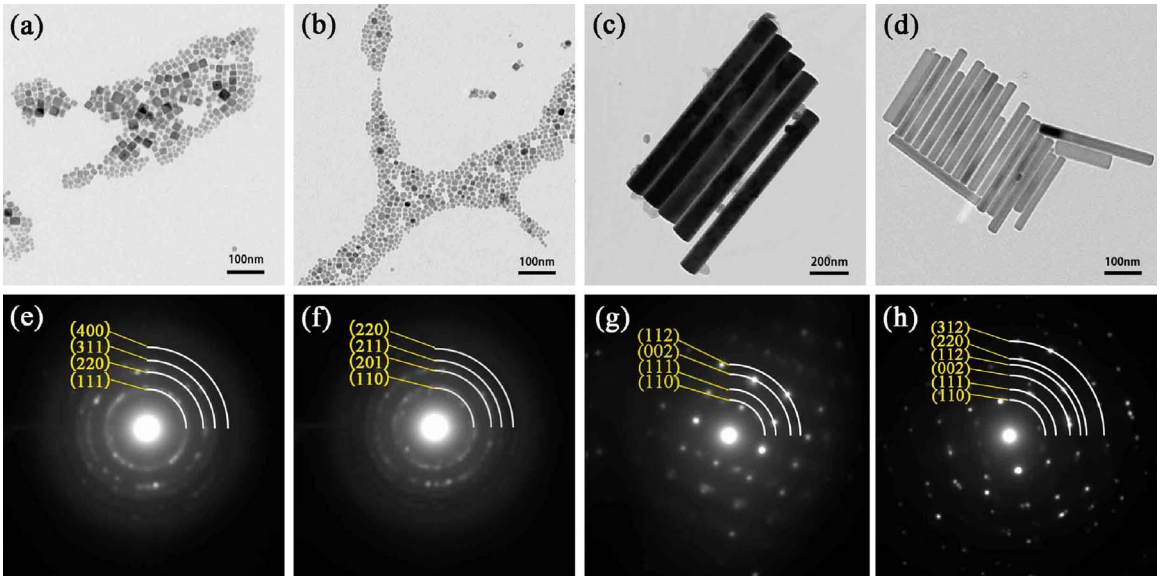

Fig. 2. TEM images of the as-prepared nanoscale samples (a) 140 °C, $NaErF_4$: 30%Yb NPs (b) 140 °C, $NaErF_4$: 30%Yb/25%Gd NPs (c) 190 °C, $NaErF_4$: 30%Yb NRs (d) 190 °C, $NaErF_4$: 30% Yb/25%Gd NRs; (e–h) the representative SAED respectively taken from (a–d).

monodispersity of all final products. At 140 °C, $NaErF_4$: 30%Yb^{3+} nanocrystals demonstrate a large quantity of nanocubes with the average granular size of 20 nm (Fig. 2a). Nevertheless, with the addition of Gd^{3+}, the particle size becomes smaller about 12 nm in diameter as shown in Fig. 2b. When the reaction temperature rises up to 190 °C, the morphology of as-synthesized samples presents clear evolution from nanocubes to nanorods. It is reasonable to believe that the reaction temperature has a prominent effect on the morphology formation process of nanostructures. In Fig. 2c, the products exhibit a uniform size with the length of about 1.05 μm and lateral diameter of about 100 nm. After doping of 25 mol% Gd^{3+}, the mean aspect ratio of NRs remains about 11 but the size decreases conspicuously (Fig. 2d). The representative SAED patterns taken from (a–d) as shown in Fig. 2(e–h) correspondingly clarify the phase transformation trend clearly, which agrees well with the aforementioned XRD results. The reduction in $NaErF_4$:Yb^{3+}, Gd^{3+} nanocrystal size partly results from the crystal surface charge modification after the substitution of lager Gd^{3+} for Er^{3+} in the crystal lattice. The increase of electron charge density on the nanocrystal surface substantially hinders the diffusion of negatively charged F^- ions to the surface due to the charge repulsion. The result consists with a previous literature [31], in which lager Eu^{3+} ions doped into $NaYF_4$ nanocrystals induces the size reduction.

The UCL properties of the as-prepared four samples with different phases and morphologies have been investigated. Fig. 3 presents the upconversion emission spectra of $NaErF_4$: 30%Yb^{3+}/xGd^{3+} (x = 0, 25 mol%) UCNCs synthesized at different synthesis temperatures under the excitation of CW 980 nm diode laser. The relatively stronger red emission bands at about 654 nm and the weaker green emission bands at about 520 nm and 540 nm, are stemming from $^4F_{9/2} \rightarrow {}^4I_{15/2}$, ($^2H_{11/2}$,$^4S_{3/2}$) $\rightarrow {}^4I_{15/2}$ transitions of Er^{3+} ions, respectively. Calculated red-to-green emission intensity ratio of four samples under different synthesis conditions has been plotted in the inset of Fig. 3. The sample S3, *i.e.* $NaErF_4$: 30%Yb^{3+} NRs, has the strongest emission intensity and the largest R/G ratio of 7.37 at the identical measurement conditions because of the relatively large size and high crystallinity. Nevertheless, the decrease in emission intensity of $NaErF_4$: 30%Yb^{3+}/25% Gd^{3+} NRs has been observed and may be resulted from the reduction in crystal size and the occurrence of cubic phase structures. On the other hand, the expansion of the distance between the Yb and Er ions because of the heavy doping level of Gd^{3+} could also be responsible for the decline of the overall upconversion luminescence intensity in NRs sample S4 compared to S3, which depresses the energy transfer rate between the sensitizers and the luminescent centers. It is interesting to note that the luminescence intensity and R/G ratio decreases sharply when the morphology changed from NRs to NPs. This can be mainly attributed to the size reduction of the nanocrystals along with the change in morphology which leads to the high surface-to-volume ratio of the UCNCs, and this is in accordance with the previous report from Murray's group [32]. However, with doping Gd^{3+} at reaction temperature of 140 °C, the emission intensity and R/G ratio of S2 are improved compared with that of S1, which is possibly ascribed to the formation of hexagonal component in $NaErF_4$:Yb^{3+}, Gd^{3+} nanostructure.

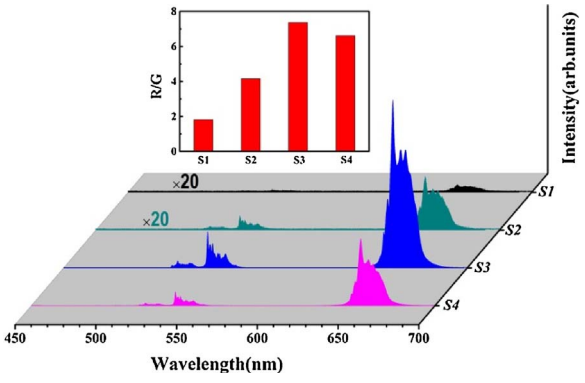

Fig. 3. Room temperature upconversion emission spectra of $NaErF_4$: 30%Yb^{3+}/xGd^{3+} (x = 0, 25 mol%) UCNCs at different synthesis temperatures under excitation with CW 980 nm diode laser. The inset presents the calculated R/G ratio of four samples.

In order to reveal the upconverting photon excitation mechanism, pumping power dependent integrated intensity of the red ($^4F_{9/2} \rightarrow {}^4I_{15/2}$) as well as green ($^2H_{11/2}$,$^4S_{3/2}$) $\rightarrow {}^4I_{15/2}$ transitions were measured and plotted in a double logarithmic scale respectively in Fig. 4(a–d) as a function of the 980 nm excitation power. In a general UC process, the relationship between UC emission intensity and the excitation power can be described by the following equation: $I_{UCL} \propto P_{NIR}{}^n$ [33,34]. Where n is the number of the required pumping photons for one upconverting emission photon, I_{UCL} is the UCL intensity, P_{NIR} is the pumping power of near infrared excitation. As displayed in Fig. 4, all corresponding slopes of the linearly fitted lines for UCL emissions at 520, 540 and 654 nm are achieved in the range of 1 to 2. This demonstrates that green and red UCL in $NaErF_4$: 30%Yb^{3+} and $NaErF_4$:

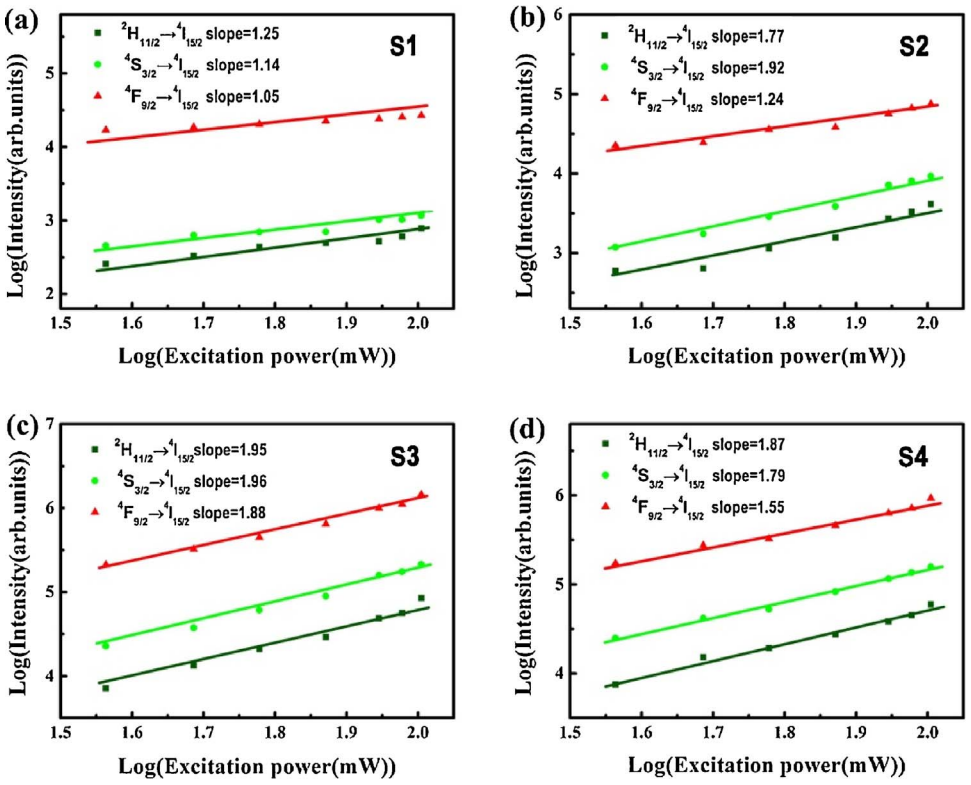

Fig. 4. Pumping power dependence plotted in the double logarithmic scales of the red ($^4F_{9/2} \rightarrow {}^4I_{15/2}$), green ($^2H_{11/2}$,$^4S_{3/2}$) $\rightarrow {}^4I_{15/2}$ UCL intensity of (a) 140 °C, $NaErF_4$: 30%Yb^{3+} NPs (b) 140 °C, $NaErF_4$: 30%Yb^{3+}/25%Gd^{3+} NPs (c) 190 °C, $NaErF_4$: 30% Yb^{3+} NRs (d) 190 °C, $NaErF_4$: 30%Yb^{3+}/25%Gd^{3+} NRs. (For interpretation of the references to colour in this figure legend, the reader is referred to the web version of this article.)

30%Yb^{3+}/25%Gd^{3+} systems follow a two photon process under the excitation of 980 nm NIR laser.

To further clarify the upconversion mechanism as well as the tailoring effect of Gd^{3+} codoping on the upconversion emissions, the transient behavior of Er^{3+}: $^2H_{11/2}$ and $^4F_{9/2}$ states for both Gd^{3+} doped and Gd^{3+}-free samples under a pulsed laser excitation of 980 nm has been intensively investigated at room temperature. Fig. 5(a) and (b) show the normalized decay profiles of the characteristic $Er^{3+}{}^2H_{11/2} \rightarrow {}^4I_{15/2}$ transition at 525 nm and $^4F_{9/2} \rightarrow {}^4I_{15/2}$ transition at 654 nm. There always exists a rise and a decay process in each transient profile of the samples, which clearly indicates the energy transfer process in this upconverting system. All the decay curves could be well fitted to double exponential function which could be simply described as: $I(t) = I_0 + A_1 e^{-t/\tau_d} - A_2 e^{-t/\tau_r}$ where $I(t)$ and I_0 are the luminescence intensities at time t and 0. A_1 and A_2 are emission intensity constants, τ_r and τ_d represent the rise and decay times of kinetics process for the exponential components, respectively. The effective decay time τ_d is determined by means of the following equation, $\tau = \frac{\int_0^\infty I(t)tdt}{\int_0^\infty I(t)dt}$, in which $I(t)$ represents the luminescence intensity at time t. The fitted upconversion lifetimes of the Er^{3+} green and red emission energy levels, *i.e.* $^2H_{11/2}$, $^4F_{9/2}$ for all the samples of Gd^{3+} doped and Gd^{3+}-free $NaErF_4$:Yb^{3+} nanostructures under the synthesis temperatures of 140 °C and 190 °C, respectively, are listed in Table 2.

Table 2
UCL lifetimes of the $^2H_{11/2}$ and $^4F_{9/2}$ states of Er^{3+} in the $NaErF_4$:Yb^{3+} NPs and NRs codoped with 0 and 25 mol% Gd^{3+}.

Sample/morphology	$^2H_{11/2}$		$^4F_{9/2}$	
	τ_r (μs)	τ_d (μs)	τ_r (μs)	τ_d (μs)
S1/NPs	1.71	11.11	8.12	34.48
S2/NPs	4.20	9.44	8.60	60.32
S3/NRs	2.52	39.95	9.30	65.81
S4/NRs	4.34	30.52	10.80	110.07

It is worth pointing out that the decay process of upconverting luminescence does not mean the depopulation of the emissive state all the time and meanwhile, the observed luminescence rise does not always represent the population of the emissive state as well, when analyzing the transient data. As a typical example, in upconverting Yb, Er codoped fluoride nanocrystals, the short τ_r components are determined by

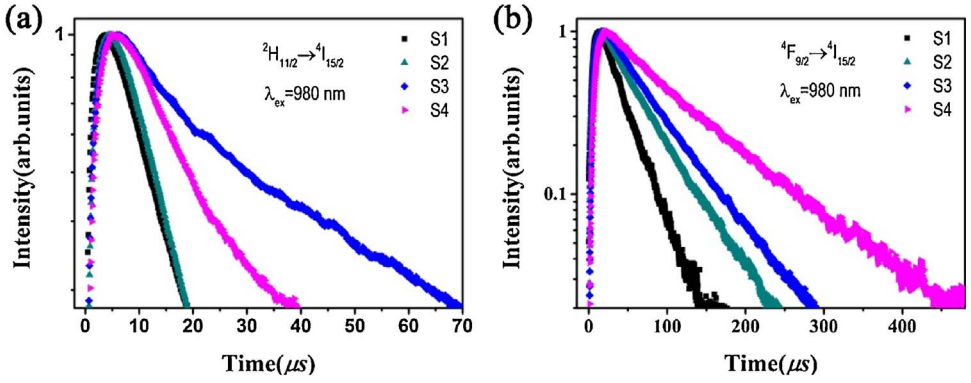

Fig. 5. Time evolutions of $NaErF_4$: 30%Yb^{3+}/xGd^{3+} (x = 0, 25 mol%) UCNCs at different synthesis temperatures by monitoring the $^2H_{11/2} \rightarrow {}^4I_{15/2}$ (a) and $^4F_{9/2} \rightarrow {}^4I_{15/2}$ (b) transitions respectively, under the excitation of a 10 ns pulsed laser at 980 nm from OPO.

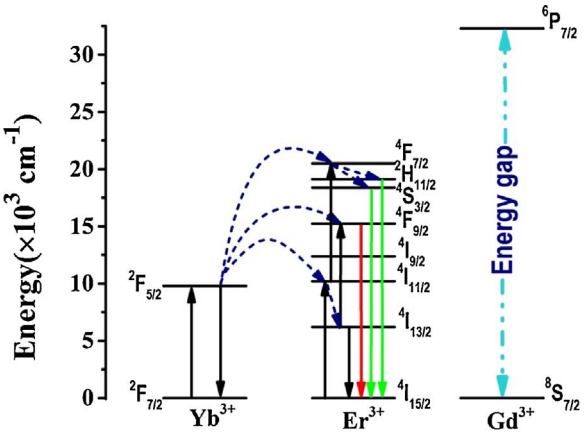

Fig. 6. Schematic energy level diagram showing the proposed upconversion mechanism of $NaErF_4$:Yb^{3+}, Gd^{3+} system.

the self-decay of emissive states $^2H_{11/2}$, $^4F_{9/2}$, therefore, they are always shorter than the decay components, even though the population on these levels is slower than the depopulation processes [35]. The longer lifetime τ_d components mainly reflect the nature of the intermediate state and determined by the product of the decay functions of the Yb^{3+}: $^2F_{5/2}$ and Er^{3+} intermediate states [36].

The decay lifetimes of red emission state Er^{3+}: $^4F_{9/2}$ in Gd^{3+}-doped $NaErF_4$:Yb NPs (sample S2) and those of the green emission state Er^{3+}: $^2H_{11/2}$ in NRs (sample S4) show a positive correlation trend to the upconversion luminescence intensity compared with those of the Gd^{3+}-free samples *i.e.* S1 and S3, respectively, as shown in Table 2. As a matter of fact, the photoluminescence lifetime of excited energy level is proportional to the inverse sum of radiative transition probability W_r and non-radiative transition probability W_n, *i.e.*$\tau \propto {}^{1}/_{(W_r + W_n)}$. Therefore, this is implying that Gd^{3+} doping could tune the W_n of the emission states since the higher non-radiative transition probability could lead to the lower emission intensity as well as the shorter decay lifetime as for the green emission in NRs. Nevertheless, for the $^2H_{11/2} \rightarrow {}^4I_{15/2}$ transition of $NaErF_4$:Yb NPs and the $^4F_{9/2} \rightarrow {}^4I_{15/2}$ transition of the NRs, the decay lifetimes of excited state exhibit a discrepancy tendency after Gd^{3+}-doping. For instance in the case of NPs, the decay lifetime of green emission state becomes shorter but the emission intensity get enhanced profoundly. One could then come to a reasonable deduction that the radiative transition probability W_r of green emission state has been greatly increased in NPs and decreased in respect of the red emission state in NRs. On the other hand, the partly released inversion symmetry and the crystal field distortion increase the electronic dipole transitions probability due to the introduction of Gd^{3+} into the crystalline lattices, which could be favorable for the enhanced UCL intensity.

The schematic energy level diagram depicting the upconversion emission process of the as-prepared samples is given in Fig. 6. In doping Gd^{3+} systems, the lowest excited level of Gd^{3+} is far higher than the excited levels of Yb^{3+} and Er^{3+}, which can perfectly avoid excitation energy loss by energy transfer between Yb^{3+}/Er^{3+} and Gd^{3+}. In the upconversion processes, the electrons are firstly excited from the $^2F_{7/2}$ level to the $^2F_{5/2}$ excited states of Yb^{3+} after absorbing the laser excitation energy at 980 nm. Then the energy transfer occurs from the excited Yb^{3+} to $Er^{3+}{}^4I_{15/2}$ ground state to populate the $^4I_{11/2}$ level. Subsequently, Yb^{3+} can further migrate excitation energy to the Er^{3+} pumping the excited electrons at $^4I_{11/2}$ to $^4F_{7/2}$ level by the excited state absorption. Excited electrons in $^4F_{7/2}$ state partly transfer to the $^2H_{11/2}$ and the $^4S_{3/2}$ states through multiphonon nonradiative relaxation steps, which consequently lead to the green emission at around 520 and 540 nm by radiative decay to the ground state. In the other way the electrons at $^4I_{11/2}$ level undergo non-radiative relaxation process to the $^4I_{13/2}$ state and then jump to $^4F_{9/2}$ level by absorbing accessional energy from Yb^{3+}. As a result, red emission around 654 nm was then generated through a radiative transition process from $^4F_{9/2}$ level to the ground state $^4I_{15/2}$ of Er^{3+}.

4. Conclusions

In summary, we have prepared $NaErF_4$:Yb^{3+},Gd^{3+} UCNCs under various experimental conditions by a facile hydrothermal route. Through tuning the synthesis temperature and Gd^{3+} doping contents the crystalline phase, morphology, size and the relative intensity of upconversion luminescence can be simultaneously controlled. Gd ions codoping could induce the partly release of inversion symmetry and the crystal field distortion, which improved the UCL efficiency as well as the R/G ratio. $NaErF_4$:Yb^{3+},Gd^{3+} nanostructures with intense red emissions show a great promising application in the biological field, particularly in *in vivo* multimodal imaging for deeper tissue penetration.

Acknowledgements

The authors greatly acknowledge the financial support from the National Natural Science Foundation of China (Nos. 11474035, 11504029, 51302019, 21502008), the Natural Science Foundation of Jilin province (20170520110JH) and 2015 programming projects on scientific research of Jilin province department of education.

References

[1] J. Shen, L. Zhao, G. Han, Lanthanide-doped upconverting luminescent nanoparticle platforms for optical imaging-guided drug delivery and therapy, Adv. Drug Deliv. Rev. 65 (2013) 744–755.
[2] Z. Gu, L. Yan, G. Tian, S. Li, Z. Chai, Y. Zhao, Recent advances in design and fabrication of upconversion nanoparticles and their safe theranostic applications, Adv. Mater. 25 (2013) 3758–3779.
[3] J. Zhou, Z. Liu, F. Li, Upconversion nanophosphors for small-animal imaging, Chem. Soc. Rev. 41 (2012) 1323–1349.
[4] L. Li, Y. Yang, R. Fan, S. Chen, P. Wang, B. Yang, W. Cao, Conductive upconversion Er, Yb-FTO nanoparticle coating to replace Pt as a low-cost and high-performance counter electrode for dye-sensitized solar cells, ACS Appl. Mater. Interfaces 6 (2014) 8223–8229.
[5] H.T. Wong, M.K. Tsang, C.F. Chan, K.L. Wong, B. Fei, J. Hao, In vitro cell imaging using multifunctional small sized $KGdF_4$: Yb^{3+} Er^{3+} upconverting nanoparticles synthesized by a one-pot solvothermal process, Nanoscale 5 (2013) 3465–3473.
[6] H. Suo, C. Guo, T. Li, Broad-scope thermometry based on dual-color modulation upconversion phosphor $Ba_5Gd_8Zn_4O_{21}$: Er^{3+}/Yb^{3+}, J. Phys. Chem. C 120 (2016) 2914–2924.
[7] T. Li, C. Guo, H. Suo, P. Zhao, Duel-mode modulation of luminescence chromaticity in $AgLa(MoO_4)_2$:Yb^{3+},Ho^{3+} up-conversion phosphors, J. Mater. Chem. C 4 (2016) 1964–1971.
[8] M. Mondal, V.K. Rai, C. Srivastava, S. Sarkar, R. Akash, Enhanced frequency upconversion in $Ho^{3+}/Yb^{3+}/Li^{+}$: $YMoO_4$ nanophosphors for photonic and security ink applications, J. Appl. Phys. 120 (2016) 233101.
[9] D.K. Chatterjee, A.J. Rufaihah, Y. Zhang, Upconversion fluorescence imaging of cells and small animals using lanthanide doped nanocrystals, Biomaterials 29 (2008) 937–943.
[10] N.M. Idris, Z. Li, L. Ye, E.K. Sim, R. Mahendran, P.C. Ho, Y. Zhang, Tracking transplanted cells in live animal using upconversion fluorescent nanoparticles, Biomaterials 30 (2009) 5104–5113.
[11] R.A. Jalil, Y. Zhang, Biocompatibility of silica coated $NaYF_4$ upconversion fluorescent nanocrystals, Biomaterials 29 (2008) 4122–4128.
[12] L. Li, K. Green, H. Hallen, S.F. Lim, Enhancement of single particle rare earth doped $NaYF_4$: Yb Er emission with a gold shell, Nanotechnology 26 (2014) 025101.
[13] Q. Dou, Y. Zhang, Tuning of the structure and emission spectra of upconversion nanocrystals by alkali ion doping, Langmuir 27 (2011) 13236–13241.
[14] F. Zhang, Q. Shi, Y. Zhang, Y. Shi, K. Ding, D. Zhao, G.D. Stucky, Fluorescence upconversion microbarcodes for multiplexed biological detection: nucleic acid encoding, Adv. Mater. 23 (2011) 3775–3779.
[15] T. Cong, Y. Ding, X. Yu, Y. Mu, X. Hong, Y. Liu, Upconversion luminescence enhancement in $NaYF_4$: Yb^{3+} Er^{3+} nanoparticles induced by Cd^{2+} tridoping, Mater. Res. Bull. 90 (2017) 151–155.
[16] Z. Wang, W. Gao, R. Wang, J. Shao, Q. Han, C. Wang, J. Zhang, T. Zhang, J. Dong, H. Zheng, Influence of SiO_2 layer on the plasmon quenched upconversion luminescence emission of core-shell $NaYF_4$: Yb Er@ SiO_2@ Ag nanocomposites, Mater. Res. Bull. 83 (2016) 515–521.
[17] J.C. Boyer, F. Vetrone, L.A. Cuccia, J.A. Capobianco, Synthesis of colloidal upconverting $NaYF_4$ nanocrystals doped with Er^{3+}, Yb^{3+} and Tm^{3+} Yb^{3+} via thermal decomposition of lanthanide trifluoroacetate precursors, J. Am. Chem. Soc. 128 (2006) 7444–7445.

[18] A.K. Soni, V.K. Rai, $BaZnLa_2O_5$:Ho^{3+}-Yb^{3+} phosphor for display and security ink application, J. Opt. Soc. Am. B 31 (2014) 2201–2207.
[19] H. Wang, W. Lu, T. Zeng, Z. Yi, L. Rao, H. Liu, S. Zeng, Multi-functional $NaErF_4$:Yb nanorods: enhanced red upconversion emission, in vitro cell, in vivo X-ray, and T_2-weighted magnetic resonance imaging, Nanoscale 6 (2014) 2855–2860.
[20] N. Niu, P. Yang, F. He, X. Zhang, S. Gai, C. Li, J. Lin, Tunable multicolor and bright white emission of one-dimensional $NaLuF_4$: Yb^{3+} Ln^{3+} (Ln = Er, tm, ho, Er/Tm, Tm/Ho) microstructures, J. Mater. Chem. 22 (2012) 10889–10899.
[21] L. Zi, D. Zhang, G. De, Self-assembly $NaGdF_4$ nanoparticles: phase controlled synthesis, morphology evolution, and upconversion luminescence properties, Mater. Res. Express 3 (2016) 025009.
[22] H. Dong, L.D. Sun, C.H. Yan, Energy transfer in lanthanide upconversion studies for extended optical applications, Chem. Soc. Rev. 44 (2015) 1608–1634.
[23] D. Ma, D. Yang, J. Jiang, P. Cai, S. Huang, One-dimensional hexagonal-phase $NaYF_4$: controlled synthesis, self-assembly, and morphology-dependent up-conversion luminescence properties, CrystEngComm 12 (2010) 1650–1658.
[24] H. Na, K. Woo, K. Lim, H.S. Jang, Rational morphology control of β-$NaYF_4$: Yb, Er/Tm upconversion nanophosphors using a ligand, an additive, and lanthanide doping, Nanoscale 5 (2013) 4242–4251.
[25] S. Zeng, G. Ren, C. Xu, Q. Yang, High uniformity and monodispersity of sodium rare-earth fluoride nanocrystals: controllable synthesis, shape evolution and optical properties, CrystEngComm 13 (2011) 1384–1390.
[26] Q. Huang, J. Yu, E. Ma, K. Lin, Synthesis and characterization of highly efficient near-infrared upconversion Sc^{3+}/Er^{3+}/Yb^{3+} tridoped $NaYF_4$, J. Phys. Chem. C 114 (2010) 4719–4724.
[27] M. Ding, C. Lu, L. Cao, Y. Ni, Z. Xu, Controllable synthesis, formation mechanism and upconversion luminescence of β-$NaYF_4$: Yb^{3+}/Er^{3+} microcrystals by hydrothermal process, CrystEngComm 15 (2013) 8366–8373.
[28] X. Wang, J. Zhuang, Q. Peng, Y. Li, A general strategy for nanocrystal synthesis, Nature 437 (2005) 121–124.
[29] F. Wang, Y. Han, C.S. Lim, Y. Lu, J. Wang, J. Xu, H. Chen, C. Zhang, M. Hong, X. Liu, Simultaneous phase and size control of upconversion nanocrystals through lanthanide doping, Nature 463 (2010) 1061–1065.
[30] X. Liang, X. Wang, J. Zhuang, Q. Peng, Y. Li, Synthesis of $NaYF_4$ nanocrystals with predictable phase and shape, Adv. Funct. Mater. 17 (2007) 2757–2765.
[31] L. Wang, Y. Li, Controlled synthesis and luminescence of lanthanide doped $NaYF_4$ nanocrystals, Chem. Mater. 19 (2007) 727–734.
[32] X. Ye, J.E. Collins, Y. Kang, J. Chen, D.T. Chen, A.G. Yodh, C.B. Murray, Morphologically controlled synthesis of colloidal upconversion nanophosphors and their shape-directed self-assembly, Proc. Natl. Acad. Sci. U. S. A. 107 (2010) 22430–22435.
[33] J.F. Suyver, J. Grimm, M.K. van Veen, D. Biner, K.W. Krämer, H.U. Güdel, Upconversion spectroscopy and properties of $NaYF_4$ doped with Er^{3+}, Tm^{3+} and/or Yb^{3+}, J. Lumin. 117 (2006) 1–12.
[34] G. Ren, S. Zeng, J. Hao, Tunable multicolor upconversion emissions and paramagnetic property of monodispersed bifunctional lanthanide-doped $NaGdF_4$ nanorods, J. Phys. Chem. C 115 (2011) 20141–20147.
[35] C. Zhao, X. Kong, X. Liu, L. Tu, F. Wu, Y. Zhang, K. Liu, Q. Zeng, H. Zhang, Li^+ ion doping: an approach for improving the crystallinity and upconversion emissions of $NaYF_4$: Yb^{3+} Tm^{3+} nanoparticles, Nanoscale 5 (2013) 8084–8089.
[36] J. Zhang, Z. Hao, J. Li, X. Zhang, Y. Luo, G. Pan, Observation of efficient population of the red-emitting state from the green state by non-multiphonon relaxation in the Er^{3+}-Yb^{3+} system, Light Sci. Appl. 4 (2015) e239.